

## Measurement of level-specific dielectronic-recombination cross sections of heliumlike Fe XXV

P. Beiersdorfer, T. W. Phillips, K. L. Wong, R. E. Marrs, and D. A. Vogel

*High Temperature Physics Division, Lawrence Livermore National Laboratory, Livermore, California 94550*

(Received 1 May 1992)

The strengths of individual  $1s2l2l'$  resonances for dielectronic recombination of heliumlike iron are measured on an electron-beam ion trap using high-resolution x-ray spectroscopy. An energy resolution  $\Delta E/E$  of better than 0.1% is achieved by monitoring the exit channel of the recombination process. Dielectronic-resonance strengths are measured relative to the cross section for nonresonant radiative electron capture of heliumlike Fe XXV, and an overall uncertainty of 20% is achieved. Good agreement with theory is found for the strongest resonances; however, less good agreement is found for the weaker resonances. The results indicate that further theoretical and experimental efforts are necessary to reliably use weak dielectronic satellite lines in plasma diagnostics.

PACS number(s): 34.80.Kw, 32.30.Rj, 52.70.La

### I. INTRODUCTION

Dielectronic recombination is the resonant capture of a free electron with the simultaneous excitation of a bound electron into a doubly excited state followed by radiative stabilization. For the 16 *KLL* resonances occurring in a heliumlike ion, i.e., electron capture into the *L* shell and concurrent excitation of a *K*-shell electron to the *L* shell, this process can be written as

$$1s^2 + e^- \rightarrow 1s2l2l' \rightarrow 1s^2 2l' + h\nu. \quad (1)$$

In hot, low-density plasmas, such as those found in the sun or in magnetic-fusion devices, dielectronic recombination is the dominant recombination mechanism of highly charged ions and is decisive in determining the charge balance [1]. The photons released in the radiative stabilization of the doubly excited, autoionizing levels populated in the resonant capture process produce a distinct signature in the x-ray spectra of few-electron, high-*Z* ions [2,3]. The intensity of these so-called dielectronic satellite lines may well exceed the intensity of characteristic lines due to electron-impact excitation. Dielectronic satellite line radiation has been observed in the x-ray spectra of many highly charged heliumlike ions, particularly the spectrum of heliumlike Fe XXV, which has been studied extensively in tokamak and solar-flare plasmas [4–9]. Because of the resonance nature of dielectronic recombination each satellite line samples a different, discrete part of the electron-energy distribution. Thus dielectronic satellite emission plays an important role in the diagnostics of hot plasmas by providing a measure of the electron temperature or by displaying the effects of a non-Maxwellian electron distribution [10–12].

The recent advent of advanced facilities for the study of atomic processes has allowed the study of dielectronic processes in unprecedented detail. For example, cross sections for dielectronic capture have been measured for heliumlike Ar XVII using the Kansas State electron-beam ion source [13,14] and for heliumlike Ni XXVII and molybdenum Mo XLI with Livermore electron-beam ion trap (EBIT) [15,16]. These measurements determined the

integrated *KLL* dielectronic-resonance strength. Individual resonances were unresolved due to the energy spread of the electron beam, which excited several resonances at once, and no level-specific cross-section measurements were made. Measurements that reveal more of the detailed structure of dielectronic resonances have been made for ions with lower charge. For example, term-specific measurements have been made of  $\Delta n = 0$  dielectronic resonances of heliumlike O VII and C V with a prototype electron cooler developed for the ASTRID storage ring in Aarhus [17,18] and of  $\Delta n = 1$  resonances of hydrogenic O VIII with the electron cooler on the heavy-ion Test Speicher Ring in Heidelberg [19]. The latter facility also provided recent results for dielectronic resonances involving the outershell electron in lithiumlike Cu XXVII [20].

In this paper we report a measurement of the dominant *KLL* dielectronic resonances of heliumlike Fe XXV on the Livermore EBIT that is level specific. Unlike previous experiments on EBIT that relied on the resolving power of the electron beam to study dielectronic resonances [15,16,21], the present measurement relies on the resolving power of a Bragg crystal spectrometer. By studying the exit channel of the dielectronic-recombination process, we can distinguish individual  $\Delta n = 1$  resonances with a resolution equal to the resolving power of the spectrometer, which in the present experiment is  $E/\Delta E = 1500$ . By contrast, the 50-eV full width at half maximum (FWHM) energy spread among beam electrons limits the resolving power to  $E/\Delta E = 90$ . The utility of high-resolution x-ray spectroscopy to study dielectronic recombination has been demonstrated in an earlier EBIT measurement of the dielectronic satellite spectra of heliumlike V XXII [22]. These measurements provided not only details about the *KLL* resonances but also about resonances involving electron capture into the  $n = 3, 4, 5$  and 6 shells [22]. However, because the measurements were not normalized, no cross sections were determined.

To normalize the present measurements and to determine the dielectronic resonance strengths, we rely on EBIT's capability to switch the electron-beam energy by

several kilovolts in less than one millisecond. Moreover, we make use of the resolving power of the electron beam to distinguish between various direct [23] and indirect [24] excitation processes that lead to x-ray emission. The normalization is accomplished by monitoring the intensity of the heliumlike transition  $1s2p\ ^1P_1 \rightarrow 1s^2\ ^1S_0$ , labeled  $w$  in the notation of Gabriel [2], to ascertain the heliumlike ion abundance, and by relating the observed dielectronic-resonance strengths to the cross section for radiative electron capture.

This paper is organized in the following way. The theoretical foundation that motivates the experimental approach is explained in Sec. II. A description of the experimental setup is presented in Sec. III. In Sec. IV we give an explanation of how we account for the angular distribution of the x-ray emission from EBIT, which arises because of the alignment of the ions in EBIT's electron beam, as well as for polarization-dependent differences in crystal reflectivities. In Sec. V we make a comparison between our measurements and theoretical predictions. Concluding remarks are presented in Sec. VI.

## II. THEORETICAL CONSIDERATIONS

The intensity  $I_s$  of a dielectronic satellite transition from autoionizing level  $|s\rangle$  to lower level  $|f\rangle$  excited by an electron beam is given by

$$I_s(E_0) = \int_{-\infty}^{+\infty} \frac{j}{e} f(E - E_0) n_{\text{He}} \sigma_s(E - E_{\text{au}}) dE. \quad (2)$$

Here  $j$  is the effective beam current density,  $e$  the electron charge, and  $n_{\text{He}}$  the number of target ions in the heliumlike ionization stage.  $f(E - E_0)$  describes the energy distribution of beam electrons, whose average kinetic energy is  $E_0$ , and

$$\int_{-\infty}^{+\infty} f(E - E_0) dE = 1. \quad (3)$$

The energy distribution of EBIT's electron beam is nearly Gaussian with a 50-eV FWHM spread; the shape of the distribution, however, does not enter subsequent calculations. Making the assumption that there is negligible interference between radiative and dielectronic recombination, which is likely to hold for iron [25,26], the energy-dependent cross section for dielectronic recombination  $\sigma_s(E - E_{\text{au}})$ , occurring at the resonance energy  $E_{\text{au}}$ , has a Lorentzian shape with a natural width that is much less than the electron-beam energy spread. The largest width for the resonances observed in this work is less than 0.5 eV. Hence it is appropriate to use the resonance strength  $S_s$

$$S_s \equiv \int_{-\infty}^{+\infty} \sigma_s(E - E_{\text{au}}) dE, \quad (4)$$

which can be expressed as

$$S_s = \frac{g_s}{g_i} \frac{A_a^{si} A_r^{sf}}{\sum_j A_a^{sj} + \sum_{f'} A_r^{sf'}} \frac{1}{E_{\text{au}}} 2\pi^2 a_0^3 \mathcal{R}^2 \left( \frac{m_e}{2\mathcal{R}} \right)^{1/2}. \quad (5)$$

$A_a^{si}$  is the autoionization rate for decay of upper level  $|s\rangle$  to the ground state  $|i\rangle$  of the recombining ion;  $A_r^{sf}$  is the

rate of radiative decay of upper level  $|s\rangle$  to lower level  $|f\rangle$ ;  $g_s$  and  $g_i$  are the statistical weights of the autoionizing level and of the ground state of the target ion, respectively. The sum over  $f'$  extends over all levels lower than  $|s\rangle$ ; the sum over  $j$  extends over all levels which are populated by autoionization of level  $|s\rangle$ ;  $m_e$  is the electron mass;  $\mathcal{R}$  and  $a_0$  are the Rydberg energy and the Bohr radius, respectively. Determining the satellite line factor  $F_2$ , which contains the satellite-specific parameters,

$$F_2 = \frac{g_s}{g_i} \frac{A_a^{si} A_r^{sf}}{\sum_j A_a^{sj} + \sum_{f'} A_r^{sf'}}, \quad (6)$$

and evaluating the constants, the resonance strength is given by

$$S_s = 2.475 \times 10^{-30} [F_2 (\text{sec}^{-1})] / [E_{\text{au}} (\text{eV})] \text{ cm}^2 \text{ eV}. \quad (7)$$

The observed satellite intensity can then be written

$$I_s(E_0) = \frac{j}{e} n_{\text{He}} S_s f(E_{\text{au}} - E_0). \quad (8)$$

The intensity of a line excited by electron impact of heliumlike ions is given by

$$I_w = \frac{j}{e} n_{\text{He}} \sigma_w. \quad (9)$$

Here  $\sigma_w$  is the cross section for electron-impact excitation. It is assumed constant across the energy spread of the electron beam. The dependence on the effective current density and the number of heliumlike ions drops out if we take the ratio of the intensity of a satellite line and a line excited by electron impact:

$$\frac{I_s(E_0)}{I_w} = \frac{S_s f(E_{\text{au}} - E_0)}{\sigma_w}. \quad (10)$$

Equation (10) forms the basis for the measurements presented in this paper. We determine the dielectronic resonance strength of a given satellite transition by measuring the dielectronic satellite intensities as a function of beam energy, normalizing each datum relative to  $w$  measured at a fixed reference energy and integrating the area under the resulting excitation function; i.e.,

$$S_s = \frac{\sigma_w}{I_w} \int_{-\infty}^{+\infty} I_s dE_0. \quad (11)$$

This method yields the dielectronic-resonance strength relative to the cross section of  $w$ . Using the procedure described by Marrs *et al.* in Ref. [23] we determine the excitation cross section of  $w$  relative to that of radiative recombination, i.e.,

$$\sigma_w = \frac{I_w}{I_{\text{RR}}} \sigma_{\text{RR}}. \quad (12)$$

Here  $I_{\text{RR}}$  is the measured x-ray intensity that stems from the radiative capture of beam electrons into the  $n=2$  shell of heliumlike ions, and  $\sigma_{\text{RR}}$  is the theoretical cross section for photon emission during the recombination process. With this procedure we normalize  $S_s$  to the

cross section for radiative recombination  $\sigma_{RR}$ . Since radiative recombination, the inverse of photoionization, involves only one electron, electron-correlation effects do not enter the calculations. Because of this, radiative-recombination cross sections are deemed to be the most accurate among the theoretical electron-ion collision cross sections. The radiative-recombination cross sections we used are calculated using the Hartree-Slater model [27,28]. Results from these calculations were compared to a large number of experimental results and were indeed found to agree with the experimental scatter for the range of electron energies we are interested in [29].

### III. EXPERIMENT

High-resolution x-ray measurements are made with EBIT's von Hámós spectrometer [30], which observes x rays in a plane of dispersion perpendicular to the electron beam. A layout of the spectrometer is shown in Fig. 1. The present measurements employed a  $12 \times 5\text{-cm}^2$  LiF(200) crystal bent to a radius of curvature  $R = 30$  cm, which provided a spectral resolving power  $\lambda/\Delta\lambda = 1500$  at a nominal Bragg angle of about  $27.5^\circ$ .

In Fig. 2 we show x-ray spectra produced at four different beam energies. The first three spectra illustrate the change in the relative intensities of various dielectronic satellite lines as the beam energy is scanned across the resonance energies. The fourth spectrum was obtained 60 eV above the threshold energy for electron-impact excitation of the heliumlike resonance line and shows the location of the four heliumlike transitions  $w$ ,  $x$ ,  $y$ , and  $z$ . At the latter electron-energy dielectronic resonances do not contribute to line excitation, and the lines seen are produced solely by electron collisions.

In order to normalize the intensity of a given dielect-

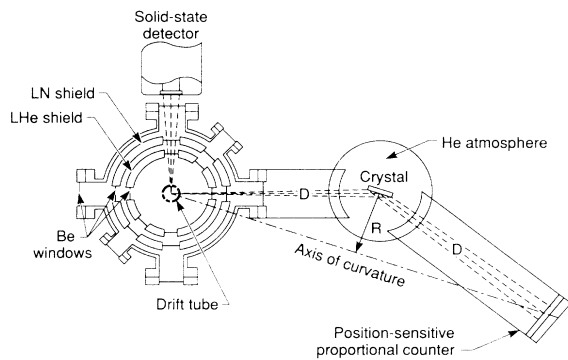


FIG. 1. Schematic diagram of the Livermore electron-beam ion trap and layout of the high-resolution von Hámós spectrometer. The electron-beam direction is out of the page. The von Hámós geometry focuses x rays in the vertical, nondispersive plane utilizing a cylindrically bent crystal. The source-to-crystal distance equals the crystal-to-detector distance. The spectrometer is filled with helium gas to reduce absorption of x rays by air. The solid-state detector is used to relate the x-ray flux produced by electron-impact excitation or dielectronic recombination to that produced by radiative recombination. LN denotes liquid-nitrogen-cooled and LHe denotes liquid-helium-cooled surfaces.

ronic satellite line to that of  $w$ , we record a spectrum of the heliumlike transitions for each satellite spectrum. For this we alternate the electron beam between the energy at which the satellites are measured and the threshold for electron-impact excitation for  $w$ . The time spent on the latter energy is short (6 msec) to minimize the varia-

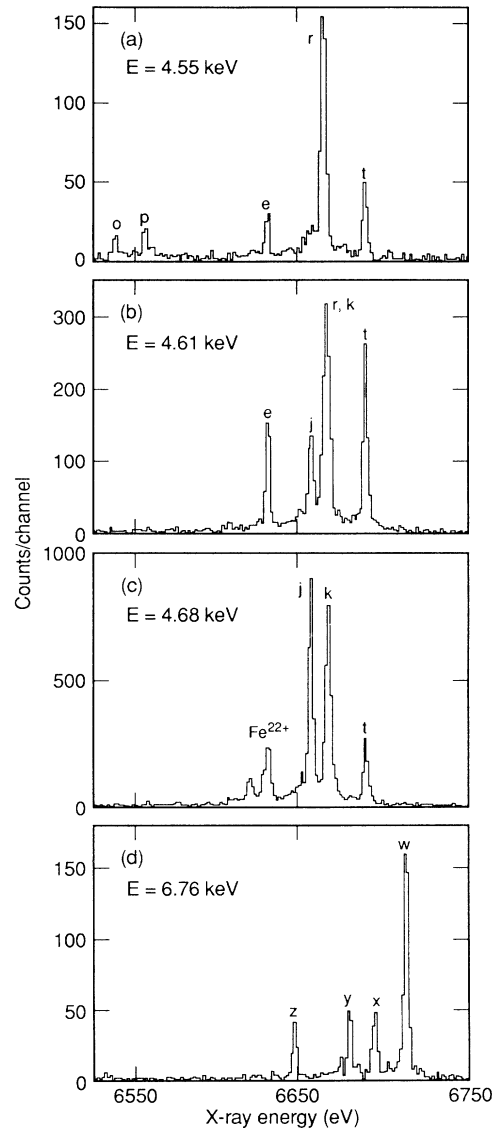


FIG. 2. Spectra of  $K$ -shell emission lines from heliumlike, lithiumlike, and berylliumlike iron recorded at different electron beam energies: (a)  $E_{\text{beam}} = 4.55$  keV; (b)  $E_{\text{beam}} = 4.61$  keV; (c)  $E_{\text{beam}} = 4.68$  keV; (d)  $E_{\text{beam}} = 6.76$  keV. The first three energies sample different parts of the  $KLL$  dielectronic resonances, and all lines are excited by dielectronic recombination. The latter energy is 60 eV above the threshold for electron-impact excitation of the heliumlike  $K$ -shell levels. This energy region is free of resonances, and all lines seen are excited directly by electron collisions. Transitions in lithiumlike iron are labeled in accordance with the key used in Table I. The heliumlike transitions are labeled  $w$ ,  $x$ ,  $y$ , and  $z$  and represent the transitions from upper levels  $1s2p\ ^1P_1$ ,  $1s2p\ ^3P_2$ ,  $1s2p\ ^3P_1$ , and  $1s2p\ ^3S_1$  to the  $^1S_0$  ground state, respectively.

tion in the charge balance. To assess the variation, we have constructed a time-dependent ionization and recombination model using theoretical cross sections for ionization, radiative, charge-exchange, and dielectronic recombination. The results of this calculation are summarized in Fig. 3, which shows the heliumlike ion abundance during the impact-excitation phase, i.e., the time the beam energy is set to measure  $w$ , relative to the heliumlike ion abundance during the recombination phase, i.e., the time dielectronic satellite spectra are observed. The model predicts that the heliumlike ion density is somewhat larger during the impact-excitation phase than during the recombination phase. This is particularly the case when the beam energy during the dielectronic-recombination phase is set to the strong resonances associated with satellites  $k$  and  $j$  (cf. Fig. 3). By normalizing the satellite intensities to that of  $w$  we thus overestimate the heliumlike ion density. Our model predicts this overestimation to be no larger than 10% when averaged over the beam energies used to determine the dielectronic-resonance strength of a particular satellite transition. To account for this overestimation, we have adjusted the measured intensities of  $w$  that enter the determination of the resonance strengths [cf. Eq. (11)] by the amounts predicted by our model. This adjustment has the effect of increasing the resultant resonance strengths by no more than 10% and adds a systematic uncertainty of no more than 6% to the determination of the resonance strengths. This is less than the uncertainty resulting from changes in the overlap of the heliumlike ions with the electron beam during the impact-excitation and dielectronic-recombination phases of the measurement. The change in this ion-beam overlap is estimated to lie between 5% and 20%, result-

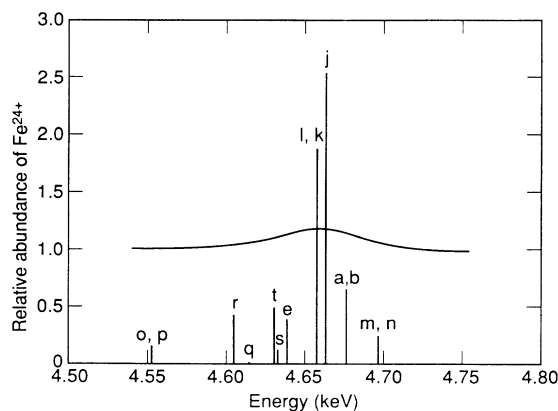


FIG. 3. Predicted abundance of heliumlike iron during the electron-impact excitation phase of the measurement relative to the heliumlike-ion abundance during the dielectronic-recombination phase. Also shown are the locations and the relative strengths of the dielectronic-recombination resonances associated with the excitation of a given set of satellite lines as calculated by Chen in Ref. [41]. The abundances of heliumlike iron are equal during the direct-excitation and dielectronic-recombination phase except near the two strong resonances associated with satellites  $l$ ,  $k$ , and  $j$ , where the relative abundance is predicted to differ as much as 10%.

ing in a 15% uncertainty in the inferred resonance strengths.

The variation of the relative intensities of several satellite lines with beam energy is shown in Fig. 4. The resonance nature of the dielectronic-recombination process is clearly evident in Fig. 4(a), which shows the variation of the intensity of dielectronic satellite  $p$ . This satellite line is produced by capture into the  $1s2s^2$  level and subsequent two-electron one-photon radiative decay to the lower level  $1s^22p_{1/2}$  [22,31]. The energy of the resonance is the lowest of any resonance of the heliumlike ion (cf. Table I and Fig. 3), and the line is situated in a spectral region well resolved from other satellite lines (cf. Fig. 2). Fitting a Gaussian function to its intensity variation we determine the energy spread in the electron beam to be 50-eV FWHM. The fit also provides us with the integrated relative line intensity for determining the resonance strength.

Satellites  $t$  and  $m$  were not resolved by our spectrometer. The calculations of Vainshtein and Safronova [32] predict their positions to be 1.8562 and 1.8565 Å, respectively, and a spectrometer with a resolving power  $\lambda/\Delta\lambda = 6200$ , four times the resolving power of our instrument, would be required to resolve these lines. The lines are produced, however, by resonances that lie 67 eV

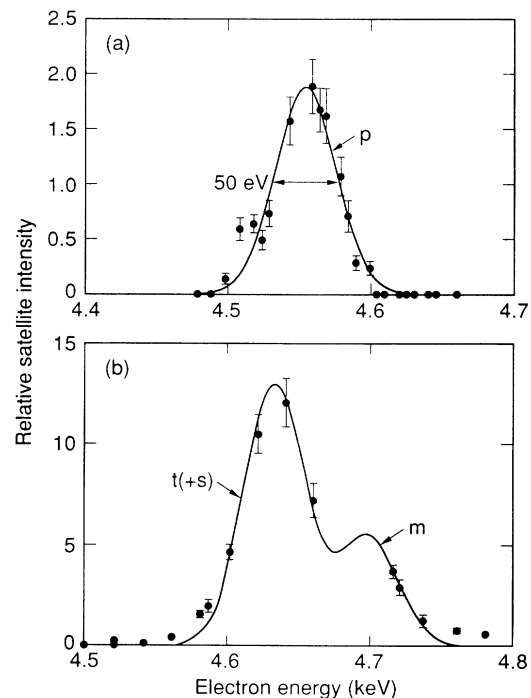


FIG. 4. Variation of the dielectronic satellite intensity with beam energy. The satellite intensities are normalized to the heliumlike resonance line  $w$  and are fitted with Gaussian profiles whose width corresponds to the energy spread of the electron beam. (a) Intensity variation of satellite  $p$ , excited by a dielectronic resonance at 4553 eV; (b) intensity variation of satellites  $t$ ,  $s$ , and  $m$ , excited by resonances at 4631, 4633, and 4698 eV, respectively. The beam energy spread is sufficiently small (50-eV FWHM) to allow separation of the contribution from  $m$ .

apart, slightly more than the spread in beam energy. A scan across their respective resonance energies does indeed reveal separate peaks, as Fig. 4(b) shows. Consequently, we can determine the integrated intensities for  $t$  and  $m$  separately. (That of  $t$  also contains a contribution from satellite  $s$ . This contribution, however, is small, as indicated in Table I.) Using similar procedures we determine the individual integrated intensities of most prominent dielectronic satellite lines. Apart from satellite  $t$ , which blends with the weak line  $s$ , the only other blended lines are  $k$ , which blends with  $a$ , and  $j$ , which blends with  $l$ .

Multiplication of the observed integrated relative satellite line intensity with  $\sigma_w$  gives the unadjusted resonance strength  $S_s^*$ ,

$$S_s^* = \frac{\sigma_w}{I_w^{\text{obs}}} \int_{-\infty}^{+\infty} I_s^{\text{obs}} dE_0. \quad (13)$$

Here  $\sigma_w$  is determined from measurements made with a solid-state detector, in accordance with Eq. (12). The measured values of  $S_s^*$  are given in Table II. We call these the unadjusted resonance strengths because the x-ray emission from interactions of ions with an electron beam is, in general, polarized [33].  $S^*$  is not identical to the resonance strength  $S$  defined in Eq. (11) without taking into account the effects of polarization on the line intensities. A detailed discussion of the effects of polarization is given in the next section.

#### IV. EFFECTS OF POLARIZATION

Before comparing the experimental results with theory we need to account for the fact that radiation from EBIT is in general linearly polarized and anisotropic. Clear evidence for the polarized nature of line radiation from EBIT was given recently by Henderson *et al.*, who ob-

TABLE I. Atomic data for the dielectronic satellite transitions  $1s^2l-1s2l^2$  in lithiumlike  $\text{Fe}^{23+}$ . Transitions are labeled in the notation of Gabriel [2].  $E_{\text{au}}$  is the dielectronic resonance energy in eV;  $P$  is the degree of linear polarization calculated by Inal and Dubau in Ref. [35];  $G(s/w)$  is the calculated crystal response factor [cf. Eq. (19)] for a particular satellite transition relative to the response to the heliumlike transition  $w$ , whose polarization is assumed to be +60%;  $S$  is the dielectronic resonance strength in units of  $10^{-20} \text{ cm}^2 \text{ eV}$ ; negative numbers in brackets indicate powers of 10. The wavelength  $\lambda$  of each transition is given in angstroms.

Key	Transition	$E_{\text{au}}$ (eV)	$\lambda(\text{\AA})^a$	$P$	$G(s/w)$	$S^a$	$S^b$	$S^c$	$S^d$
$a$	$(1s2p_{3/2}^2)_{3/2} \rightarrow 1s^22p_{3/2}$	4677.0	1.8617	$-\frac{3}{4}$	0.14	8.11	6.40	6.24	6.88
$b$	$(1s2p_{1/2}^2)_{3/2} \rightarrow 1s^22p_{1/2}$	4677.0	1.8573	$\frac{3}{5}$	1.00	0.11	0.13	0.08	0.09
$c$	$(1s2p_{1/2}2p_{3/2})_{1/2} \rightarrow 1s^22p_{3/2}$	4658.6	1.8667	0	0.68	0.02	0.02	0.04	0.03
$d$	$(1s2p_{1/2}2p_{3/2})_{1/2} \rightarrow 1s^22p_{1/2}$	4658.6	1.8623	0	0.68	0.07	0.07	0.13	0.08
$e$	$(1s2p_{1/2}2p_{3/2})_{5/2} \rightarrow 1s^22p_{3/2}$	4639.0	1.8721	$\frac{1}{2}$	0.93	4.80	4.28	4.12	4.32
$f$	$(1s2p_{1/2}2p_{3/2})_{3/2} \rightarrow 1s^22p_{3/2}$	4632.9	1.8738	$-\frac{3}{4}$	0.14	0.20	0.26	0.09	0.16
$g$	$(1s2p_{1/2}2p_{3/2})_{3/2} \rightarrow 1s^22p_{1/2}$	4632.9	1.8694	$\frac{3}{5}$	1.00	4.5[-4]	4.0[-3]	4.1[-4]	5.6[-4]
$h$	$(1s2p_{1/2}^2)_{1/2} \rightarrow 1s^22p_{3/2}$	4624.6	1.8761	0	0.68	1.8[-4]	2.1[-4]	1.0[-4]	1.0[-4]
$i$	$(1s2p_{1/2}^2)_{1/2} \rightarrow 1s^22p_{1/2}$	4624.6	1.8717	0	0.68	0.04	0.02	0.02	0.03
$j$	$(1s2p_{3/2}^2)_{5/2} \rightarrow 1s^22p_{3/2}$	4664.1	1.8654	$\frac{1}{2}$	0.93	29.15	27.22	26.27	26.90
$k$	$(1s2p_{1/2}2p_{3/2})_{3/2} \rightarrow 1s^22p_{1/2}$	4658.1	1.8625	$\frac{3}{5}$	1.00	19.60	18.60	17.27	17.53
$l$	$(1s2p_{1/2}2p_{3/2})_{3/2} \rightarrow 1s^22p_{3/2}$	4658.1	1.8669	$-\frac{3}{4}$	0.14	2.32	1.79	2.22	2.22
$m$	$(1s2p_{3/2}^2)_{1/2} \rightarrow 1s^22p_{3/2}$	4697.7	1.8562	0	0.68	2.91	2.56	2.44	2.41
$n$	$(1s2p_{3/2}^2)_{1/2} \rightarrow 1s^22p_{1/2}$	4697.7	1.8519	0	0.68	0.13	0.09	0.12	0.11
$o$	$(1s2s^2)_{1/2} \rightarrow 1s^22p_{3/2}$	4553.4	1.8963	0	0.68	0.84	0.91	0.82	0.94
$p$	$(1s2s^2)_{1/2} \rightarrow 1s^22p_{1/2}$	4553.4	1.8918	0	0.68	0.85	0.92	0.80	0.91
$q$	$(1s2s2p_{3/2})_{3/2} \rightarrow 1s^22s_{1/2}$	4615.3	1.8605	$\frac{3}{5}$	1.00	0.11	0.02	0.12	2.0[-3]
$r$	$(1s2s2p_{1/2})_{1/2} \rightarrow 1s^22s_{1/2}$	4604.9	1.8630	0	0.68	3.13	3.62	4.45	3.68
$s$	$(1s2s2p_{3/2})_{3/2} \rightarrow 1s^22s_{1/2}$	4633.2	1.8557	$\frac{3}{5}$	1.00	0.15	0.90	0.67	0.24
$t$	$(1s2s2p_{3/2})_{1/2} \rightarrow 1s^22s_{1/2}$	4631.2	1.8565	0	0.68	6.35	5.83	5.28	5.77
$u$	$(1s2s2p_{1/2})_{3/2} \rightarrow 1s^22s_{1/2}$	4570.1	1.8732	$\frac{3}{5}$	1.00	0.17	0.02	0.04	0.15
$v$	$(1s2s2p_{1/2})_{1/2} \rightarrow 1s^22s_{1/2}$	4566.3	1.8743	0	0.68	0.03	0.02	0.01	2.9[-3]

<sup>a</sup>Vainshtein and Safronova, Ref. [32].

<sup>b</sup>Bely-Dubau, *et al.*, Ref. [40].

<sup>c</sup>Chen, Ref. [41].

<sup>d</sup>Nilsen, Ref. [42].

TABLE II. Comparison of measured dielectronic-resonance strengths with theoretical values.  $S^*$  represents the observed resonance strength in units of  $10^{-20} \text{ cm}^2 \text{ eV}$ , uncorrected for the crystal response and angular distribution.  $R$  is defined as the ratio of the theoretical resonance strength given in Table I and the measured resonance strength adjusted by the crystal response factor  $G(s/w)$  from Table I, i.e.,  $R = SG(s/w)/S^*$ . The estimated absolute uncertainty in the experimental values, including the spectrometer response factor, is about 20%; the relative uncertainty is about 13%.

Key	$S^*$	$R^a$	$R^b$	$R^c$	$R^d$
$e$	3.63	1.23	1.10	1.06	1.11
$j(+l)$	24.06	1.15	1.06	1.03	1.05
$k(+a)$	21.23	0.98	0.93	0.86	0.87
$m$	1.52	1.31	1.14	1.10	1.08
$r$	3.42	0.62	0.72	0.89	0.73
$t(+s)$	3.65	1.22	1.33	1.17	1.14
$o$	0.48	1.20	1.29	1.16	1.34
$p$	0.50	1.16	1.26	1.10	1.25

<sup>a</sup>Value of  $S$  based on atomic data from Vainshtein and Safronova, Ref. [32].

<sup>b</sup>Value of  $S$  based on atomic data from, Bely-Dubau *et al.*, Ref. [40].

<sup>c</sup>Value of  $S$  based on atomic data from Chen, Ref. [41].

<sup>d</sup>Value of  $S$  based on atomic data from Nilsen, Ref. [42].

served the  $K$ -shell emission of heliumlike Sc XIX [34]. The effect of polarization needs to be accounted for in the evaluation of lines excited both by dielectronic electron capture and by electron impact. Polarization affects our measurement in two ways. First, because of the anisotropy in the line emission the x-ray intensity  $I(90^\circ)$  observed along the spectrometer axis at  $90^\circ$  to the beam direction differs from the  $4\pi$ -averaged intensity  $\langle I \rangle$ . Second, the analyzing crystal in the spectrometer acts as a polarizer and preferentially reflects x rays polarized parallel to the beam direction.

For electric dipole radiation, i.e., for the type of radiation we are concerned with in this measurement, the relationship between the x-ray emission observed perpendicular to the beam  $I(90^\circ)$  and its space-averaged value  $\langle I \rangle$  is [33]

$$I(90^\circ) = \frac{3}{3-P} \langle I \rangle. \quad (14)$$

$P$  is the linear polarization, defined as the fractional difference between the intensity of light with electric-field vector parallel to the beam direction  $I_{\parallel}$  and the intensity of light with electric-field vector perpendicular  $I_{\perp}$ :

$$P = \frac{I_{\parallel} - I_{\perp}}{I_{\parallel} + I_{\perp}}, \quad (15)$$

where

$$I_{\parallel} + I_{\perp} = I(90^\circ). \quad (16)$$

The x-ray intensity  $I^{\text{obs}}$  observed with our crystal spectrometer differs from  $I(90^\circ)$ , however, because the crystal reflects the two field components differently. Defining  $f_{\parallel}$  and  $f_{\perp}$  as the integrated crystal reflectivities for x rays

polarized parallel and perpendicular to the plane of dispersion,  $I^{\text{obs}}$  is given by

$$I^{\text{obs}} = f_{\parallel} I_{\parallel} + f_{\perp} I_{\perp}. \quad (17)$$

Using Eqs. (14)–(17) the intensity ratio of two observed lines can be related to their  $4\pi$ -averaged values via the expression

$$\frac{I_1^{\text{obs}}}{I_2^{\text{obs}}} = G \left[ \frac{1}{2} \right] \frac{\langle I_1 \rangle}{\langle I_2 \rangle}, \quad (18)$$

where we have defined a relative spectrometer response factor  $G$  that accounts for the dependence of the crystal reflectivity on linear polarization as well as for the anisotropy of each line,

$$G \left[ \frac{1}{2} \right] \equiv \frac{f_{\parallel}^1(1+P_1) + f_{\perp}^1(1-P_1)}{f_{\parallel}^2(1+P_2) + f_{\perp}^2(1-P_2)} \frac{3-P_2}{3-P_1}. \quad (19)$$

Once we have determined the spectrometer response factor we can determine the dielectronic resonance strength  $S_s$  of a particular satellite  $s$  from the observed resonance strength  $S_s^*$ , defined in Eq. (13), by writing

$$S_s = S_s^* / G \left[ \frac{s}{w} \right]. \quad (20)$$

In the present experiment we have not measured the line polarization and angular distribution, or the crystal reflectivities, but we use instead theoretical values for these quantities.

For spin-zero target ions the polarization and angular distribution of the dielectronic-recombination x rays are given by angular momentum coupling coefficients and depend only on the spin of the resonance level  $|s\rangle$  and of the lower level  $|f\rangle$  populated in the radiative stabilization, as discussed recently by Inal and Dubau [35]. An overview of the linear polarization of each satellite transition is given in Table I. In an earlier paper Inal and Dubau discussed the polarization of the heliumlike transitions excited by electron impact [36]. The degree of polarization of collisionally excited lines varies as a function of electron energy. Inal and Dubau calculate  $P_w = 58.4\%$  for the iron  $w$  line at threshold [36]. Similarly, using the values of the magnetic sublevel populations calculated by Zhang, Sampson, and Clark [37], we determine  $P_w = 60\%$  for the beam energy (6.76 keV) at which we measure  $w$ . Finally, to account for the crystal response to polarized radiation we rely on the results of Gullikson [38], who has made detailed calculations of the integrated crystal reflectivities for linearly polarized x rays. Combining the information on line polarization and crystal reflectivities, we have calculated the spectrometer response to each satellite line  $s$  relative to that of  $w$ . A summary of the values of  $G(s/w)$  is given in Table II. Note that  $G(s/w)$  does not exceed unity. This is because the spectrometer preferentially records positively polarized x rays and the polarization of none of the satellite lines exceeds that of  $w$ .

It is important to stress that  $G$  does not vary strongly with changes in either  $P_w$ ,  $f_{\perp}$ , or  $f_{\parallel}$ . For example, a 10% uncertainty in the crystal response translates into a 3.3%

uncertainty for the value of  $G(w/s)$ , if  $s$  is unpolarized. The uncertainty is smaller if  $s$  is positively polarized; but it is somewhat larger if  $s$  is negatively polarized. Similarly, a change in  $P_w$  by 10% results in a 4.2% change in  $G$ . The uncertainty in our theoretical estimates of the line polarization is well below this value. However, the EBIT electron beam has a transverse temperature, which has the effect of spreading the incident electron direction, and thus of reducing the degree of polarization of the emitted radiation. Furthermore, a rigid rotor motion of the beam adds to the transverse motion. As a result, the polarization may be reduced by 0.5–1.5% from our estimated value, adding an estimated 1% to the uncertainty in  $G$ .

## V. COMPARISON WITH THEORY

A large body of theoretical data exists pertaining to the dielectronic satellite emission of Fe XXIV. The data include rates for radiative decay and autoionization of the doubly excited lithiumlike levels along with transition energies, which we can use to calculate the resonance strength, Eq. (7). In the following we compare our measured resonance strengths to the values we derived from the atomic-data calculations of Vainshtein and Safronova [32], Bely-Dubau *et al.* [39,40], Chen [41], and Nilsen [42]. A summary of the derived resonance strengths is given in Table I. Here we list the resonance strengths associated with each of the 22 dipole-allowed x-ray transitions originating from one of 15 autoionizing levels populated by a *KLL* resonance and terminating in one of the three ground-state levels of the lithiumlike ion. The resonance strength of the autoionizing level  $1s2s2p^4P_{5/2}$ , which cannot decay by dipole-allowed transitions but decays instead by an electric quadrupole transition, is not listed.

Inspection of Table I shows close agreement among the various theoretical calculations for the strong resonances associated with transitions  $j$  and  $k$ . Less close agreement among the various theoretical results is found for satellite transitions associated with resonances with intermediate strengths. For example, the spread in the calculated resonance strength leading to satellite  $r$  is 40%, that associated with  $a$  is 30%. Even larger variations are found for the smallest resonances; the predictions for satellite  $s$  vary by a factor of 6, that for satellite  $u$  by a factor of 8, and that for  $q$  by a factor of more than 60.

Our measurements are sensitive enough to test resonances as small as  $5 \times 10^{-21} \text{ cm}^2 \text{ eV}$ , e.g., the resonances that produce the satellite transitions  $o$  and  $p$ . A comparison between the resonance strengths observed in our experiment and the various theoretical predictions is made in Table II, which lists the ratio of each predicted value to our observed resonance strength associated with each observed dielectronic transition,

$$R = S_s G \left[ \frac{s}{w} \right] / S_s^* . \quad (21)$$

Here we multiply the predicted strength by the spectrometer response factor  $G(s/w)$ ; for resonances unresolved in the measurement the numerator is the sum over each

contributing resonance multiplied by the predicted response factor.

Perfect agreement between theory and experiment corresponds to  $R = 1$ . The absolute uncertainty of the experimental value, including the spectrometer response factor, is about 20% and is dominated by uncertainties in the relative change of the ion-beam overlap between the dielectronic-recombination and the direct-excitation phases of the measurement. As a result, only values of  $R$  smaller than 0.80 or larger than 1.20 fall outside the error limits. Consequently, the data are in good agreement with all calculations for the resonance strengths associated with  $j$  and  $k$ . This is important because these two resonances overwhelmingly dominate the total dielectronic-recombination strength of the *KLL* resonances. Previous experiments, which measured the total strength of the *KLL* resonance, also agreed with theory within a 10–15% error limit [13–16]. However, there are several values of  $R$  that fall outside the error limits pointing to disagreements with theory. For example, the value for satellite  $r$  calculated with the resonance strength predicted by Vainshtein and Safronova [32] is only 0.62, indicating that the predicted resonance strength is too small; the value of 1.31 for satellite  $m$ , which indicates a resonance strength predicted too large by the calculations of Vainshtein and Safronova [32]; as well as the values for  $o$  and  $p$ , whose resonance strengths are predicted too large by the calculations of Bely-Dubau *et al.* [40] and Nilsen [42].

While the absolute error of our measurements is about 20%, the relative error limits are only about 13%. Thus we can better assess the relative accuracy of predictions. Inspection of Table II shows, for example, that most calculations underestimate the size of  $r$  relative to that of  $j$ . Overall, we find best agreement between our measurements and the calculations of Chen [41], who has used a multiconfigurational Dirac-Fock approach; our data differ most from the calculations of Vainshtein and Safronova [32], who have used a *Z*-expansion method.

## VI. CONCLUSION

We have presented level-specific measurements of the strengths of  $1s2l2l'$  dielectronic resonances in iron by studying the exit channel in the recombination process with high-resolution x-ray spectroscopy. The resolution that we have attained with this method is about 4.5 eV, a resolving power of  $\Delta E/E = 0.1\%$ . This betters the resolution of 54 eV achieved [15,16] by using EBIT's electron beam to resolve the resonances of heliumlike nickel and the 19-eV resolution achieved more recently [43] by using ion-extraction techniques to study the dielectronic resonances of hydrogenlike argon.

Theoretical predictions for the strong dielectronic resonances are in good mutual agreement, and our measurements affirm the accuracy of these predictions. Less agreement exists among theoretical predictions for the size of intermediate-strength resonances. Our measurements distinguish between several of these predictions. Overall, our measurements agree best with the calculations of Chen [41], who uses a multiconfiguration Dirac-

Fock approach.

The theoretical values for the weakest dielectronic resonances vary tremendously. The accuracy of the calculation of their resonance strengths depends sensitively on the accuracy of the wave functions constructed for determining weak radiative or Auger rates. The present measurements are not sensitive enough to test the accuracy of the various approaches used in the calculations of the weakest resonances. Recent experiments, however, have shown that some of the weakest resonances, such as that producing satellite  $u$ , can be observed with high-resolution x-ray spectroscopy [31]. Future measurements tailored specifically to determine the strengths of the weakest resonances will undoubtedly distinguish among the widely diverging theoretical predictions. Such measurements, together with further theoretical efforts, are undoubtedly needed to improve the reliability of the determinations of plasma parameters from the intensity

of the dielectronic satellite emission associated with weak- or intermediate-strength resonances.

#### ACKNOWLEDGMENTS

We are grateful for the expert technical support of D. Nelson and E. Magee as well as for the encouragement received from Dr. A. Hazi and Dr. M. Eckart. Discussions with Dr. M. H. Chen are greatly appreciated. We also thank Dr. E. Källne for lending us the detector used in the measurements and Dr. E. Gullikson for providing us with his calculations on crystal reflectivities before their publication. This work was supported in part by NASA under Contract No. NAGW-2688 and was performed under the auspices of the U. S. Department of Energy by the Lawrence Livermore National Laboratory under Contract No. W-7405-ENG-48.

- 
- [1] A. Burgess, *Astrophys. J.* **139**, 776 (1964).  
 [2] A. H. Gabriel, *Mon. Not. R. Astron. Soc.* **160**, 99 (1972).  
 [3] J. Dubau and S. Volonté, *Rep. Prog. Phys.* **43**, 199 (1980).  
 [4] Yu. I. Grineva, V. I. Karev, V. V. Korneev, V. V. Krutov, S. L. Mandelstam, L. A. Vainshtein, B. N. Vasilyev, and I. A. Zhitnik, *Sol. Phys.* **29**, 441 (1973).  
 [5] G. A. Doschek, R. W. Kreplin, and U. Feldman, *Astrophys. J.* **233**, L157 (1979).  
 [6] K. W. Hill, S. von Goeler, M. Bitter, L. Campbell, R. D. Cowan, B. Fraenkel, A. Greenberger, R. Horton, J. Hovey, W. Roney, N. R. Sauthoff, and W. Stodieck, *Phys. Rev. A* **19**, 1770 (1979).  
 [7] M. Bitter, K. W. Hill, N. R. Sauthoff, P. C. Efthimion, E. Merservey, W. Roney, S. von Goeler, R. Horton, M. Goldman, and W. Stodieck, *Phys. Rev. Lett.* **43**, 129 (1979).  
 [8] G. A. Doschek, U. Feldman, and R. D. Cowan, *Astrophys. J.* **245**, 315 (1981).  
 [9] J. F. Seely, U. Feldman, and U. I. Safronova, *Astrophys. J.* **304**, 838 (1986).  
 [10] F. Bely-Dubau, M. Bitter, J. Dubau, P. Faucher, A. H. Gabriel, K. W. Hill, S. von Goeler, N. Sauthoff, and S. Volonté, *Phys. Lett.* **93A**, 189 (1983).  
 [11] R. Bartiromo, F. Bombarda, and R. Giannella, *Phys. Rev. A* **32**, 531 (1985).  
 [12] J. F. Seely, U. Feldman, and G. A. Doschek, *Astrophys. J.* **319**, 541 (1987).  
 [13] R. Ali, C. P. Bhalla, C. L. Cocke, and M. Stockli, *Phys. Rev. Lett.* **64**, 633 (1990).  
 [14] R. Ali, C. P. Bhalla, C. L. Cocke, M. Schulz, and M. Stockli, *Phys. Rev. A* **44**, 223 (1991).  
 [15] D. A. Knapp, R. E. Marrs, M. A. Levine, C. L. Bennett, M. H. Chen, J. R. Henderson, M. B. Schneider, and J. H. Scofield, *Phys. Rev. Lett.* **62**, 2104 (1989).  
 [16] D. Knapp, *Z. Phys. D* **21**, S143 (1991).  
 [17] L. H. Andersen, P. Hvelplund, H. Knudsen, and P. Kvistgaard, *Phys. Rev. Lett.* **62**, 2656 (1989).  
 [18] L. H. Andersen, J. Bolko, and P. Kvistgaard, *Phys. Rev. A* **41**, 1293 (1990).  
 [19] G. Kilgus, J. Berger, P. Blatt, M. Grieser, D. Habs, B. Hochadel, E. Jaeschke, D. Krämer, R. Neumann, G. Neureither, W. Ott, D. Schwalm, M. Steck, R. Stokstad, E. Szmola, A. Wolf, R. Schuch, A. Müller, and M. Wagner, *Phys. Rev. Lett.* **64**, 737 (1990).  
 [20] A. Wolf, J. Berger, M. Bock, D. Habs, B. Hochadel, G. Kligus, G. Neureither, U. Schramm, D. Schwalm, E. Szmola, A. Müller, M. Wagner, and R. Schuch, *Z. Phys. D* **21**, S69 (1991).  
 [21] M. B. Schneider, D. A. Knapp, M. H. Chen, J. H. Scofield, P. Beiersdorfer, C. Bennett, J. R. Henderson, M. A. Levine, and R. E. Marrs, *Phys. Rev. A* **45**, R1291 (1992).  
 [22] P. Beiersdorfer, M. H. Chen, R. E. Marrs, M. B. Schneider, and R. S. Walling, *Phys. Rev. A* **44**, 396 (1991).  
 [23] R. E. Marrs, M. A. Levine, D. A. Knapp, and J. R. Henderson, *Phys. Rev. Lett.* **60**, 1715 (1988).  
 [24] P. Beiersdorfer, A. L. Osterheld, M. H. Chen, J. R. Henderson, D. A. Knapp, M. A. Levine, R. E. Marrs, K. J. Reed, M. B. Schneider, and D. A. Vogel, *Phys. Rev. Lett.* **65**, 1995 (1990).  
 [25] N. R. Badnell, M. S. Pindzola, and D. C. Griffin, *Phys. Rev. A* **43**, 2250 (1991).  
 [26] N. R. Badnell and M. S. Pindzola, *Phys. Rev. A* **45**, 2820 (1992).  
 [27] J. H. Scofield, *Phys. Rev. A* **40**, 3054 (1989).  
 [28] J. H. Scofield, *Phys. Rev. A* **44**, 139 (1991).  
 [29] E. B. Saloman, J. H. Hubbell, and J. H. Scofield, *At. Data Nucl. Data Tables* **38**, 1 (1988).  
 [30] P. Beiersdorfer, R. E. Marrs, J. R. Henderson, D. A. Knapp, M. A. Levine, D. B. Platt, M. B. Schneider, D. A. Vogel, and K. L. Wong, *Rev. Sci. Instrum.* **61**, 2338 (1990).  
 [31] P. Beiersdorfer, M. H. Chen, S. MacLaren, R. E. Marrs, D. A. Vogel, K. Wong, and R. Zasadzinski, *Phys. Rev. A* **44**, 4730 (1991).  
 [32] L. A. Vainshtein and U. I. Safronova, *At. Data Nucl. Data Tables* **25**, 49 (1978).  
 [33] I. C. Percival and M. J. Seaton, *Philos. Trans. R. Soc. London Ser. A* **251**, 113 (1958).  
 [34] J. R. Henderson, P. Beiersdorfer, C. L. Bennett, S. Chantrenne, D. A. Knapp, R. E. Marrs, M. B. Schneider, K. L. Wong, G. A. Doschek, J. F. Seely, C. M. Brown, R. E. LaVilla, J. Dubau, and M. A. Levine, *Phys. Rev. Lett.* **65**, 705 (1990).  
 [35] M. K. Inal and J. Dubau, *J. Phys. B* **22**, 3329 (1989).

- [36] M. K. Inal and J. Dubau, *J. Phys. B* **20**, 4221 (1987).
- [37] H. L. Zhang, D. H. Sampson, and R. E. H. Clark, *Phys. Rev. A* **41**, 198 (1990).
- [38] E. M. Gullikson (private communication).
- [39] F. Bely-Dubau, A. H. Gabriel, and S. Volonté, *Mon. Not. R. Astron. Soc.* **186**, 405 (1979).
- [40] F. Bely-Dubau, J. Dubau, P. Faucher, and A. H. Gabriel, *Mon. Not. R. Astron. Soc.* **198**, 239 (1982).
- [41] M. H. Chen, *At. Data Nucl. Data Tables* **34**, 301 (1986).
- [42] J. Nilsen, *At. Data Nucl. Data Tables* **38**, 339 (1988).
- [43] D. R. DeWitt, D. Schneider, M. W. Clark, M. H. Chen, and D. Church, *Phys. Rev. A* **44**, 7185 (1991).